Monochromatic 2D Kα Emission Images Revealing Short-Pulse Laser Isochoric Heating Mechanism

H. Sawada, Y. Sentoku, T. Yabuuchi, U. Zastrau, E. Förster, F. N. Beg, H. Chen, A. J. Kemp, H. S. McLean, P. K. Patel, and Y. Ping

Phys. Rev. Lett. **122**, 155002 — Published 18 April 2019

DOI: 10.1103/PhysRevLett.122.155002

Monochromatic 2D Kα emission images revealing short-pulse laser isochoric heating mechanism

H. Sawada[1], Y. Sentoku[2], T. Yabuuchi[3], U. Zastrau[4], E. Förster[5,6], F. N. Beg[7], H. Chen[8], A. J. Kemp[8], H. S. McLean[8], P. K. Patel[8] and Y. Ping[8]

[1] *University of Nevada Reno, Reno, NV, USA*
[2] *Institute of Laser Engineering, Osaka University, Suita, Japan*
[3] *RIKEN SPring-8 Center, Hyogo, Japan*
[4] *European XFEL, Schenefeld, Germany*
[5] *IOQ, Friedrich-Schiller University of Jena, Jena, Germany*
[6] *Helmholtz Institute at Jena, Jena, Germany*
[7] *University of California San Diego, La Jolla, USA*
[8] *Lawrence Livermore National Laboratory, Livermore, CA, USA*

The rapid heating of a thin titanium foil by a high intensity, sub-picosecond laser is studied by using a 2D narrow-band x-ray imaging and x-ray spectroscopy. A novel monochromatic imaging diagnostic tuned to 4.51 keV Ti Kα was used to successfully visualize a significantly ionized area (<Z> >17±1) of the solid density plasma to be within a ~ 35 μm diameter spot in the transverse direction and 2 μm in depth. The measurements and a 2D collisional Particle-in-cell simulation reveal that, in the fast isochoric heating of solid foil by intense laser light, such high ionization state in the solid titanium is achieved by thermal diffusion from the hot preplasma in a few picoseconds after the pulse ends. The shift of Kα and formation of a missing Kα cannot be explained with the present atomic physics model. The measured Kα image is reproduced only when a phenomenological model for the Kα shift with a threshold ionization of <Z>=17 is included. This work reveals how the ionization state and electron temperature of the isochorically-heated non-equilibrium plasma are independently increased.

Keywords:

PACS:

With high-intensity, short-pulse lasers, matter can be heated to extremely high temperature and pressure states within the time scale of a few picoseconds, while the density is maintained near solid. This rapid heating known as isochoric heating[1,2,3] has a potential to efficiently create hot solid density plasmas that can be a vital testbed for studies of equation of state[4,5], thermal conductivity[6], opacity[7,8,9] and stopping power of high-energy ions including α-particles[10], and to serve as compact radiation/neutron sources[11,12] or ignitor of a dense fusion fuel for fast ignition (FI) laser fusion[13].

In a laser-solid interaction at a peak intensity of > 10^{18} W/cm^2, energetic (fast) electrons predominantly accelerated by ponderomotive potential play a central role in transferring the laser energy to the target. Three major heating mechanisms associated with fast electrons are identified: resistive heating, drag heating and diffusion.[14,15] Propagation of forward-going fast electrons in dense plasmas draws an equal current of cold electrons in the opposite direction. This cold return current resistively heats the background plasma via collisional dissipation. The propagating fast electrons also lose energy via direct collisions with the background electrons (drag heating). In a small foil (< 1 mm^2), fast electrons recirculate due to sheath potentials developed on the foil surfaces, supplying its own return current. Thus, the resistive heating becomes no longer efficient when the recirculation starts. Heating by diffusion occurs via thermal conduction due to a temperature gradient between a hot plasma and a cold region.

Despite extensive research on isochoric heating of thin solid targets over the last two decades, there is no consensus on the dominant heating mechanism among resistive heating[16,17,18,19,20], drag heating[21,22,23,24,25,26,27,28], diffusion[1,3,29], and both drag and resistive heating[30,31,32,33,34]. The current puzzle is that bulk electron temperatures (T_e) estimated span a wide range from tens of eV to 5 keV[35] at similar laser and target conditions. In the most experiments, T_e is inferred from analyses of x-ray emission spectra with collisional-radiative atomic physics codes including fast electrons as a non-thermal component of the temperature distribution (T_{hot}). However, the x-ray diagnostic is interfered by hot preplasma and has not been benchmarked against other diagnostic techniques.

Isochoric heating of high density plasma has been performed for FI where a dense fuel core is ignited by drag heating with MeV electrons. In current integrated FI experiments[36,37,38], enhancement of fusion neutron yields is observed with the injection of an ignitor laser, however, the heating mechanism is not understood well. Understanding of the heating mechanisms in solids or dense plasmas requires spatially and temporally resolved diagnostics as well as benchmarked modeling in atomic physics and a particle-in-cell (PIC) code for non-equilibrium plasmas.

This Letter reports an investigation of an isochorically heated thin titanium foil using spatially and spectrally resolved x-ray measurements and a 2D collisional PIC code PICLS[39]. A novel monochromatic crystal imager was developed to provide an ionization map of the foil for the first time. Together with the PIC simulation incorporating a dynamic ionization model, the results reveal that the ionization state, <Z>, and T_e of the foil are independently increased by different mechanisms associated with MeV electrons, followed by significant thermal diffusion.

A series of experiments was conducted using a 50 TW laser Leopard[40] at Nevada Terawatt Facility. It delivered the energy of 1-16 J in a pulse with a 350 fs full width at half maximum (FWHM) at the wavelength of λ=1057 nm. Figure 1 shows a layout of the experiment. The beam was tightly focused with a f/1.5 off-axis parabolic mirror on a 2 or 10 μm thick titanium foil mounted on a glass stalk. The measured spot image in Fig.1 (b) was analyzed to estimate a ~8 μm diameter spot containing 30% of the laser energy. The pedestal prior to the main pulse was measured with fast photodiodes to be of the order of 10^8 and ~ 1 ns long. This is reasonable because the same system was used to consistently produce a proton beam with the maximum energy of ~ 10 MeV by irradiating 2 μm titanium foils for proton deflectometry.[41] On a single target shot, escaped fast electrons, x-ray spectrum and a monochromatic x-ray image were simultaneously recorded in the target rear with a magnet-based electron spectrometer[42], a Bragg crystal spectrometer and a spherical crystal imager, respectively.

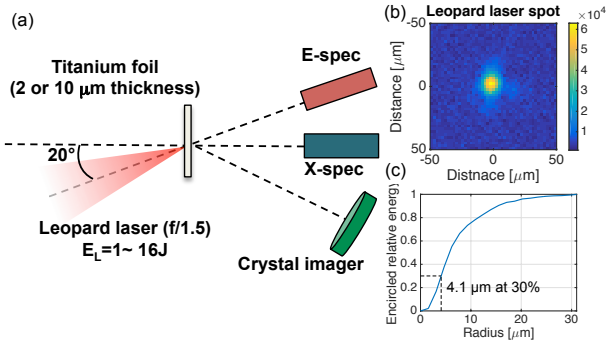

Figure 1 (a) A Leopard laser experimental setup. (b) Measured focal spot. (c) Encircled beam energy

Table 1 A summary of laser energies and target types

Shot	Laser Energy	Thickness	Foil surface area
(A)	3.8 J	2 μm	500 × 500 μm^2
(B)	16.0 J	2 μm	800 × 500 μm^2
(C)	16.0 J	2 μm	125 × 80 μm^2
(D)	16.0 J	10 μm	300 × 200 μm^2

Kα had a magnification of 10 and a spatial resolution of 12±1 μm. The spectral bandwidth of the imager is calculated to be 5 eV based on the imager configuration.[43]

Target heating was studied by varying foil types and laser energies as summarized in Table.1. Data were taken at least three times for each shot and target condition. Figure 2

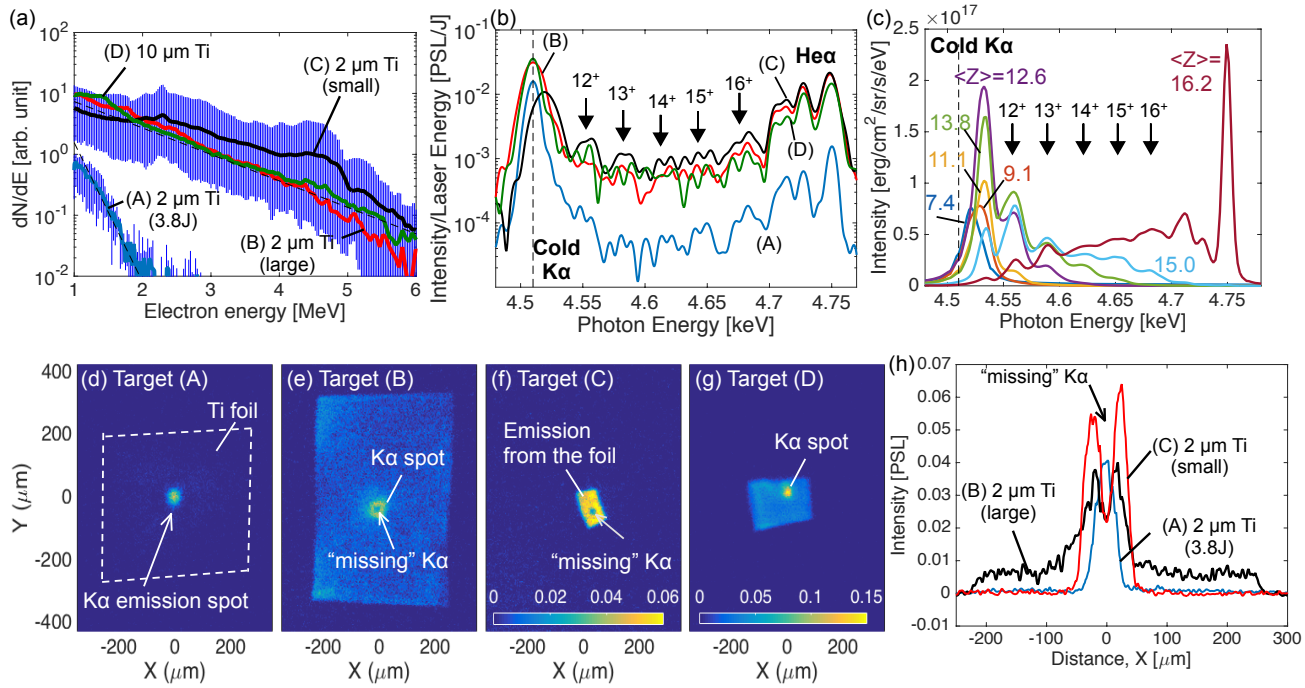

Figure 2 (a) Measured escaped electron spectra, (b) x-ray spectra, (c) atomic physics modeling of cold and shifted Kα emissions with PrismSPECT, (d) ~ (g) 4.51 keV monochromatic x-ray images for shots (A) ~ (D). (h) Lineouts of the Kα images for shots (A)~ (C)

The crystal imager configured to image 4.51 keV cold Ti shows measured electron spectra, x-ray spectra, 2D

monochromatic Kα images for shots (A) ~ (D) and calculated x-ray spectra with PrismSPECT[44]. The electron measurement in Fig.2 (a) is important to characterize fast electron spectrum with a slope temperature (T_{hot}) without using scaling laws[45,46,47]. The slope is correlated to the electron spectrum generated at the laser interaction point.[48] Additionally, changes in the slope indicate shot-to-shot variations due to target mispositioning and surface conditions. The measured slope was fit with an exponential function to be $T_{hot} = 0.19 \pm 0.06$ MeV and 1.30 ± 0.40 MeV at 3.8 J and 16 J, respectively. The higher laser energy increases not only T_{hot}, but also the number of fast electrons substantially in the MeV range. Similar slopes observed with ~16 J for (B)~(D) and all other shots taken throughout the campaigns ensure that fast electron generation is comparable regardless of the surface areas and the foil thicknesses. The experimental T_{hot} is used to validate input parameters for a PIC simulation presented later, similarly in Ref. 49.

Fig.2 (b) shows background-subtracted x-ray spectra normalized by the laser energy. Distinct spectral peaks of cold Kα at 4.51 keV and Heα lines at ~4.75 keV were observed for all shots, while a series of so-called shifted Kα[50] between cold Kα and Heα lines, originated in Kα transitions from ionized titanium ions (Ti^{12+} ~ Ti^{16+}), was recorded for shots (B) and (C). The observation of the shifted Kα is a clear indication of solid density, ionized plasma.[51] Calculations of ionization-dependent shifted Kα are performed in the range of T_e between 100 and 400 eV with fast electrons having a non-Maxwellian temperature of 1.5 MeV and the number density fraction of 5%. The results are insensitive to the choice of the fast electron parameters ranging from 1 to 5 % density fraction and from 0.2 to 2.0 MeV. Blue-shifts of the Kα line peak from 4.51 keV are seen at $\langle Z \rangle = 7 \sim 9$. At above $\langle Z \rangle \sim 12$, where all M-shell electrons are removed, the spectrum shows multiple peaks of shifted Kα. Qualitatively, $\langle Z \rangle$ of ~16 is required to reproduce the measured spectrum. In this calculation, the ionization of the plasma is driven not only by thermal electrons, but also by fast electrons via electron impact ionization.[44] Therefore, the emission spectra cannot be an accurate representation of T_e. Further discussions on the origin of the measured lines and the calculated x-ray spectra for various T_e and $\langle Z \rangle$ are presented in the Supplemental Material[525354].

The spectral shift of cold Kα due to ionization changes affects imaging data recorded with a narrow-band spherically bent crystal. Such crystals have been applied for forming quasi-monochromatic images of cold Kα emissions.[55,56,57,58,59] Here, by taking advantage of the bandwidth narrowness, the crystal imager was used to identify the area of a strongly ionized plasma by measuring a reduction of cold Kα due to ionization increase. An atomic physics calculation shows that the signal on the imager increases up to $\langle Z \rangle = 12$ when line shift and spectral shape are taken into account. This numerical investigation is presented in the Supplemental Material.[6061]

Figure 2 (d-g) show 4.51 keV monochromatic x-ray images.[62] The yield of Kα emissions is proportional to the number of fast electrons colliding with K-shell electrons of the background ions, while the spatial extent of the emission depends on the fast electron energy. At the low energy shot (A), Fig.2 (d) shows an emission spot with a 47 μm FWHM in diameter and faint signals from the foil surface indicated by dotted lines. When the laser energy is increased from 4 to 16 J, the number of MeV electrons is significantly increased and a monochromatic image for shot (B) in Fig.2 (e) clearly shows three distinct features: Kα spot near the laser interaction, Kα emission from the entire foil, and a dip inside the Kα spot here called "missing" Kα signal. MeV electrons, whose the continuous slowing down approximation (CSDA)[63] ranges are of the order of a few millimeters, recirculate around the foil multiple times and induce relatively uniform emission from the entire foil except the edges and the Kα spot. The formation of the Kα spot and the missing Kα, which are created by diffusion, will be discussed later.

To examine the role of the MeV electrons in target heating, a foil with a smaller surface area (125x80 μm^2) as displayed in Fig.2 (f) was used to increase the interaction of the fast electrons with the foil. Due to the enhanced recirculation in the limited surface area, the surface emission was increased compared to the large foil and overwhelmed a Kα spot, creating a uniform surface emission except the area of the missing Kα. However, the size and depth of the missing Kα are comparable between the large and small foils as compared in Fig.2 (h). Since strong ionization could widen the missing Kα, the result suggests that further thermal ionization driven by an increase of T_e due to drag heating does not occur even in the small foil, contradicting with past results reporting that a high temperature plasma is created by reducing a target volume[22,25,28,30,34,64]. We discuss potential misinterpretation of the measurements and provide an alternative explanation for Kα spectral analysis in the Supplemental Material[65].

The depth of heating into the foil was investigated by changing the thickness of foils from 2 to 10 μm. The x-ray image for the 10 μm foil shows a Kα spot and higher surface emission, but no missing Kα. This image further supports that creation of the missing Kα is not due to drag heating with the MeV electrons that can penetrate into a 1 mm thick Cu foil. Therefore, the comparison of the images for these foils implies that the depth of the strongly ionized region is less than 10 μm, and Kα emission produced in the deeper layer (2 ~ 10 μm depth) may overcome the dip.

Formation of the missing Kα is considered as a consequence of spectral line shift due to strong ionization. Alternative interpretations could be due to (1) prepulse drilling a hole in the foil, (2) main pulse pushing ions away, or (3) line shifts caused by high plasma density, strong electric or magnetic fields. A laser drilling creates a hole with depth-to-diameter ratio > 1.[66] The interpretation for the case (1) is discarded because the diameter of the missing Kα is ~35 μm, but the dip is observed only in the 2 μm thick foil. For the case (2), the main pulse must push

more than 50% of the ions in the center away to observe the dip. However, a PIC simulation suggests that a density decrease at the center of the foil is ~ 1% at 2 ps. The interpretation for the case (3) is unlikely because the Kα line whose outer shells are filled is insusceptible to modifications of the ionic potential. The shifts of spectral lines due to a high density has been observed in low-Z, 1s-2p Lyman transition[3,67,68].

To understand the dynamics of solid target heating including formation of Kα spot and missing Kα with fast electrons, two-dimensional collisional PIC simulations are performed using the PICLS code. The simulation shown in Fig.3 is run up to 2.0 ps in a 135×200 μm^2 system box with absorbing boundaries, where fast electrons escape so the simulation corresponds to the large target. A 2-μm thick titanium layer is placed between X = 22 and 24 μm. The laser pulse peaks at 0.3 ps with a 350 fs FWHM and ends at ~ 0.6 ps. A more detail of the code and setup is described in the Supplemental Material[6970].

Figure 3 (a) ~ (f) show average ionization contours and line profiles of <Z> and T_e averaged over the foil. The preplasma is ionized to high charge states (> ~17) as the laser propagates up to the critical density at X= ~13 μm. The fast electrons mainly accelerated at the critical density propagate through the overdense preplasma (X=13~22 μm) and the solid foil. After reaching the target rear, the electrons recirculate and transversely propagate around the foil, ionizing the central region of the foil uniformly up to <Z> ~ 12 as shown in Fig.3 (a) and (e) at 0.5 ps. The electron temperature, on the other hand, is increased only near the center of the foil in Fig.3 (f). This is caused by resistive heating during the fast electron transport to the target rear and it is no longer effective once the electrons reach the rear surface because they supply their own return current. As a result, electron recirculation creates non-equilibrium plasma where the spatial profiles of <Z> and T_e are deviated.

Significant target heating above <Z> ~ 12 and T_e > 70 eV occurs predominantly by diffusion after the laser pulse ends. Fig.3 (g) shows the phase space of electrons and ions along Y = 50 μm at 1.5 ps. The resistive heating heats the solid as well as the overdense preplasma, creating a T_e gradient at the interface and driving diffusive heating into the solid at ~ 1 ps. The evidence of the diffusion is seen in the gradient of the electron energies at X= ~22 μm in Fig.3 (g). The solid foil is continuously heated by the diffusion, but the increase of T_e in the solid foil becomes slower as the T_e gradient between the preplasma and the solid foil becomes smaller. A more discussion including the phase maps at different times and T_e profiles along the X direction is presented in the Supplemental Material[71].

Fast ions, accelerated by the sweeping potential toward the solid foil[72], also deposit their energy in the foil. However, the contribution of the ions to the target temperature is concluded to be minimal because (1) the ions do not reach the foil at 1.0 ps when the heating begins and (2) the spread of the fast ion beam penetrating through the foil is smaller than the ionized area by the electrons.

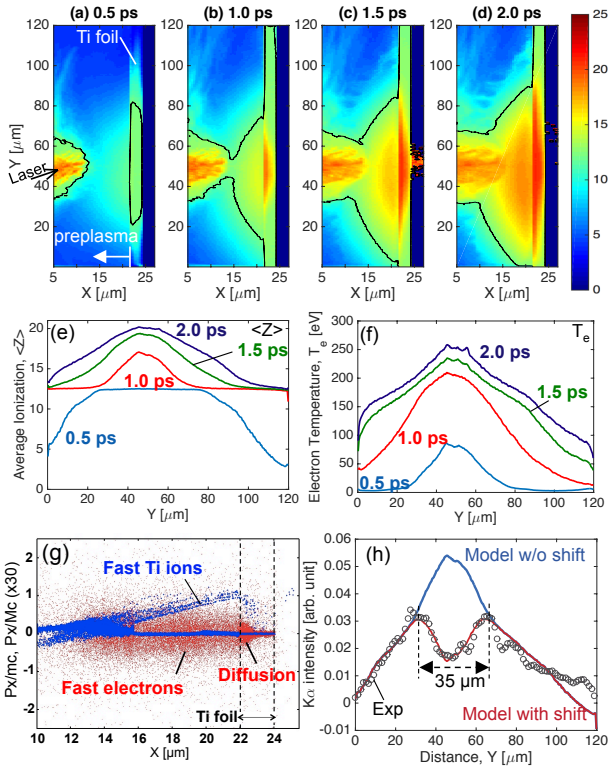

Figure 3 (a~d) Ionization contours at 0.5, 1.0, 1.5 ps and 2.0 ps. Temporal evolutions of (e) <Z> and (f) T_e profiles. (g) Phase space of fast electrons and ions at 1.5 ps. (h) Comparisons of the measured Ka profile to calculations with and without the effect of the Ka shift.

Fig.3 (h) compares a lineout of the measured Kα image for shot (B) in Fig.2 (e) with integrated ionization profiles. The width of the Kα spot is in good agreement with the time-integrated profile without the effect of Kα shift. A slight deviation in X > ~70 μm is most likely due to the target positioning inaccuracy. To incorporate ionization-dependent Kα shift for the imaging data, a phenomenological signal reduction model based on a step function is used. By post-processing the PIC-calculated ionization profiles with this model, the time-integrated profile is in excellent agreement with the measurement in Fig.3 (h) when the model uses a threshold ionization parameter of <Z> = 17±1 and the integration time up to 1.5 ps. The spatial extent above <Z> = 17 in the PIC simulation is 33.6 μm at 1.5 ps, which is consistent with the opening of the measured missing Kα. A model for shifted Kα using PrismSPECT overestimates the decay above <Z> = 12 and does not reproduce the measured Kα spot. Note that the model used to reproduce the missing Kα is not a physics-based modeling so that development and benchmarking of an atomic-physics-based Kα shift model are necessary. The Supplemental Material presents details of these models and how the threshold <Z> and integration times are determined.[73]

The present results provide new insights into understanding isochoric heating of thin solid foils with sub-picosecond lasers, which could clarify past contradicting results. Most importantly, a short-pulse laser-irradiated foil must be considered to be in non-equilibrium state where <Z> and T_e are increased independently. The

monochromatic images reflect spatial distribution of time-integrated ionization states driven by both fast electrons and diffusive thermal electrons as shown by the PIC simulation. The fast electron recirculation increases the ionization that is observed in the increased Kα yields in the small foil. However, it does not increase T_e to the temperature, which ionizes further and expands the size of the missing Kα. The high charge states is explained by the diffusive thermal electrons arriving to the target after the pulse ends. This result suggests that the use of Kα yields or Kα spectra as a T_e diagnostic could be misinterpretation of data because (1) Kα emission correlates to <Z>, not T_e, and (2) Kα photons can be produced by both non-thermal and a high-energy tail of thermal electrons. Because of the above reasons, care must be taken when Kα yields are used to estimate coupling efficiency from laser to a compressed core[74,75] for FI at moderately high densities where drag heating is ineffective ($n_e < \sim 10^{25}$ [1/cm^3]).

In conclusion, the experimental evidence of isochoric heating of a thin titanium foil with an intense sub-picosecond laser is presented. A novel narrow-band crystal imager was successfully applied for the first time for visualizing ionization map of the solid foil, providing unprecedented constraints on isochoric heating. This work reveals that resistive heating and diffusion are the dominant heating mechanisms, whereas drag heating does not contribute to heating of the solid foil. The crystal imaging of missing Kα could be applied for high ionization state measurements. The findings of the isochoric heating mechanisms and the non-equilibrium state of the plasma in the present work could open up new opportunities and directions in high energy density physics and fusion energy research with short-pulse lasers.

This work was partially supported by DOE/OFES under Contract No. DE-SC0008827, DOE/Cooperative Agreement under contact No. DE-NA0002075, and the JSPS KAKENHI under Grant number JP15K21767. H.S. would like to acknowledge Dr. P. Wiewior, O. Chalyy, A. Astanovitskiy, O. Dmitriev, V. Nalajala, V. Davis and the NTF management for their support of the Leopard laser experiments.

[1] Z. Jiang, J.C. Kieffer, J.P. Matte, M. Chaker, O. Peyrusse, D. Gilles, G. Korn, A. Maksimchuk, S. Coe, and G. Mourou, Phys. Plasmas 2, 1702 (1995)
[2] J. Workman, A. Maksimchuk, X. Liu, U. Ellenberger, J.S. Coe, C.-Y. Chien, and D. Umstadter, Phys. Rev. Lett. 75, 2324 (1995).
[3] A. Saemann, K. Eidmann, I. E. Golovkin, R. C. Mancini, E. Andersson, E. Förster, and K. Witte, Phys. Rev. Lett. 82, 4843 (1999)
[4] P. K. Patel, A. J. Mackinnon, M. H. Key, T. E. Cowan, M. E. Foord, M. Allen, D. F. Price, H. Ruhl, P. T. Springer, and R. Stephens, Phys. Rev. Lett. 91, 125004 (2003)
[5] G.M. Dyer, A.C. Bernstein, B.I. Cho, J. Osterholz, W. Grigsby, A. Dalton, R. Shepherd, Y. Ping, H. Chen, K. Widmann, and T. Ditmire, Phys. Rev. Lett. 101, 015002 (2008)
[6] A. McKelvey, G.E. Kemp, P.A. Sterne, A. Fernandez-Panella, R. Shepherd, M. Marinak, A. Link, G.W. Collins, H. Sio, J. King *et al*., Sci. Rep. 7, 7015 (2017).
[7] P. Audebert, R. Schepherd, K. B. Fournier, O. Peyrusse, D. Price, R. Lee, R. Springer, J.C. Gauthier, and L. Klein, Phys.Rev.Lett. 89, 265001 (2002)
[8] P. Audebert, P. Renaudin, S. Bastiani-Ceccotti, J.-P. Geindre, C. Cheanis- Popovics, S. Tzortzakis, V. Nagels-Silvert, R. Shepherd, I. Matsushima, S. Gary, et al., Phys. Rev. Lett. 94, 025004 (2005)
[9] S. N. Chen, G. Gregori, P. K. Patel, H.-K. Chung, R. G. Evans, R. R. Freeman, E. Garcia Saiz, S. H. Glenzer, S. B. Hansen, F. Y. Khattak *et al*., Phys. Plasmas 14, 102701 (2007).
[10] J.A. Frenje, P.E. Grabowski, C.K. Li, F.H. Séguin, A.B. Zylstra, M. Gatu Johnson, R.D. Petrasso, V.Y. Glebov, and T.C. Sangster, Phys. Rev. Lett. 115, 205001 (2015).
[11] J. Workman, M. Nantel, A. Maksimchuk, and D. Umstadter, Appl. Phys. Lett. **70**, 312 (1998).
[12] Y. Sentoku, A.J. Kemp, R. Presura, M.S. Bakeman, and T.E. Cowan, Phys. Plasmas 14, 122701 (2007).
[13] M. Tabak, J. Hammer, M.E. Glinsky, W. L. Kruer, S.C. Wilks, J. Woodworth, E.M. Campbell, M.D. Perry, and R. J. Mason, Phys. Plasmas 1, 1626 (1994).
[14] A.J. Kemp, Y. Sentoku, V. Sotnikov, and S.C. Wilks, Phys. Rev. Lett. 97, 235001 (2006)
[15] P. Norreys, D. Batani, S. Baton, F.N. Beg, R. Kodama, P.M. Nilson, P. Patel, F. Pérez, J.J. Santos, R.H.H. Scott, V.T. Tikhonchuk, M. Wei, and J. Zhang, Nucl. Fusion 54, 054004 (2014).
[16] C.R.D. Brown, D.J. Hoarty, S.F. James, D. Swatton, S.J. Hughes, J.W. Morton, T.M. Guymer, M.P. Hill, D. A. Chapman, J.E. Andrew *et al*., Phys. Rev. Lett. 106, 185003 (2011)
[17] M. Storm, B. Eichman, C. Orban, S. Jiang, G. Fiksel, C. Stoeckl, G. Dyer, T. Ditmire, R. Stephens, W. Theobald, J.A. Delettrez, R.R. Freeman, and K. Akli, Phys. Plasmas 21, 72704 (2014).
[18] V. Dervieux, B. Loupias, S. Baton, L. Lecherbourg, K. Glize, C. Rousseaux, C. Reverdin, L. Gremillet, C. Blancard, V. Silvert, et al., High Energy Density Phys. 16, 12 (2015).
[19] E.V. Marley, R. Shepherd, P. Beiersdorfer, G. Brown, H. Chen, J. Dunn, M. Foord, H. Scott, R. London, A.B. Steel *et al*., High Energy Density Phys. 25, 15 (2017).
[20] K.L. Lancaster, A.P.L. Robinson, J. Pasley, P. Hakel, T. Ma, K. Highbarger, F.N. Beg, S.N. Chen, R.L. Daskalova, R.R. Freeman *et al*., Phys. Plasmas 24, 83115 (2017).
[21] S. Hansen, A. Faenov, T. Pikuz, K. Fournier, R. Shepherd, H. Chen, K. Widmann, S. Wilks, Y. Ping, H.K. Chung, A. Niles, J.R. Hunter, G. Dyer, and T. Ditmire, Phys. Rev. E 72, 036408 (2005).
[22] S.D. Baton, M. Koenig, P. Guillou, B. Loupias, A. Benuzzi-Mounaix, J. Fuchs, C. Rousseaux, L. Gremillet, D. Batani, A. Morace, M. Nakatsutsumi, R. Kodama, and Y. Aglitskiy, High Energy Density Phys. 3, 358 (2007).
[23] P.M. Nilson, W. Theobald, J. Myatt, C. Stoeckl, M. Storm, O. V. Gotchev, J.D. Zuegel, R. Betti, D.D. Meyerhofer, and T.C. Sangster, Phys. Plasmas 15, 56308 (2008)
[24] P.M. Nilson, W. Theobald, J.F. Myatt, C. Stoeckl, M. Storm, J.D. Zuegel, R. Betti, D.D. Meyerhofer, and T.C. Sangster, Phys. Rev. E 79, 016406 (2009).
[25] P. Neumayer, H.J. Lee, D. Offerman, E. Shipton, A. Kemp, A.L. Kritcher, T. Döppner, C.A. Back, and S.H. Glenzer, High Energy Density Phys. 5, 244 (2009)
[26] F. Perez, L. Gremillet, M. Koenig, S.D. Baton, P. Audebert, M. Chahid, C. Rousseaux, M. Drouin, E. Lefebvre, T. Vinci, et al., Phys. Rev. Lett. 104, 085001 (2010)
[27] U. Zastrau, P. Audebert, V. Bernshtam, E. Brambrink, T. Kämpfer, E. Kroupp, R. Loetzsch, Y. Maron, Y. Ralchenko, H. Reinholz, et al., Phys. Rev. E 81, 026406 (2010).
[28] P.M. Nilson, A. A. Solodov, J.F. Myatt, W. Theobald, P. A. Jaanimagi, L. Gao, C. Stoeckl, R.S. Craxton, J. A. Delettrez, B. Yaakobi, et al., Phys. Plasmas 18, 056703 (2011).
[29] O.N. Rosmej, Z. Samsonova, S. Höfer, D. Kartashov, C. Arda, D. Khaghani, A. Schoenlein, S. Zähter, A. Hoffmann, R. Loetzsch, A. Saevert, I. Uschmann, M.E. Povarnitsyn, N.E. Andreev, L.P. Pugachev, M.C. Kaluza, and C. Spielmann, Cit. Phys. Plasmas 25, 83103 (2018).
[30] G. Gregori, S.B. Hansen, R. Clarke, R. Heathcote, M.H. Key, J. King, R.I. Klein, N. Izumi, A.J. Mackinnon, S.J. Moon *et al*., Contrib. to Plasma Phys. 45, 284 (2005).
[31] E. Martinolli, M. Koenig, S.D. Baton, J.J. Santos, F. Amiranoff, D. Batani, E. Perelli-Cippo, F. Scianitti, L. Gremillet, R. Mélizzi, et al., Phys. Rev. E 73, 046402 (2006).

[32] J.J. Santos, A. Debayle, P. Nicolaï, V. Tikhonchuk, M. Manclossi, D. Batani, A. Guemnie-Tafo, J. Faure, V. Malka, and J.J. Honrubia, Eur. Phys. J. Spec. Top. 175, 71 (2009).
[33] H. Nishimura, R. Mishra, S. Ohshima, H. Nakamura, M. Tanabe, T. Fujiwara, N. Yamamoto, S. Fujioka, D. Batani, M. Veltcheva, et al., Phys. Plasmas 18, 022702 (2011).
[34] P. Neumayer, B. Aurand, R.A. Costa Fraga, B. Ecker, R.E. Grisenti, A. Gumberidze, D.C. Hochhaus, A. Kalinin, M.C. Kaluza, T. Kühl, et al., Phys. Plasmas 19, 122708 (2012).
[35] K.U. Akli, S.B. Hansen, A.J. Kemp, R.R. Freeman, F.N. Beg, D.C. Clark, S.D. Chen, D. Hey, S.P. Hatchett, K. Highbarger, et al., Phys. Rev. Lett. 100, 165002 (2008).
[36] R. Kodama, P.A. Norreys, K. Mima, A.E. Dangor, R.G. Evans, H. Fujita, Y. Kitagawa, K. Krushelnick, T. Miyakoshi, N. Miyanaga, et al., Nature 412, 798 (2001).
[37] W. Theobald, A.A. Solodov, C. Stoeckl, K.S. Anderson, R. Betti, T.R. Boehly, R.S. Craxton, J.A. Delettrez, C. Dorrer, J.A. Frenje, et al., Phys. Plasmas 18, 056305 (2011).
[38] H. Shiraga, S. Fujioka, M. Nakai, T. Watari, H. Nakamura, Y. Arikawa, H. Hosoda, T. Nagai, M. Koga, H. Kikuchi, et al., EPJ Web Conf. 59, 01008 (2013).
[39] Y. Sentoku and A.J. Kemp, J. Comput. Phys. 227, 6846 (2008)
[40] P.P. Wiewior, V. V Ivanov, and O. Chalyy, J. Phys. Conf. Ser. 244, 032013 (2010).
[41] D. Mariscal, C. McGuffey, J. Valenzuela, M.S. Wei, J.P. Chittenden, N. Niasse, R. Presura, S. Haque, M. Wallace, A. Arias, et al., Appl. Phys. Lett. 105, 224103 (2014).
[42] H. Chen, A.J. Link, R. van Maren, P.K. Patel, R. Shepherd, S.C. Wilks, and P. Beiersdorfer, Rev. Sci. Instrum. **79**, 10E533 (2008)
[43] T. Missalla, I. Uschmann, E. Förster, G. Jenke, and D. von der Linde, Rev. Sci. Instrum. 70, 1288 (1999)
[44] J.J. MacFarlane, I.E. Golovkin, P.R. Woodruff, D. R. Welch, B.V. Oliver, T.A. Mehlhorn and R.B. Campbell, Proceedings of Inertial Fusion and Science Applications 2003
[45] S. C. Wilks, W. L. Kruer, M. Tabak, and A. B. Langdon, Phys. Rev. Lett. 69, 1383 (1992)
[46] F. N. Beg, A. R. Bell, A. E. Dangor, C. N. Danson, A. P. Fews, M. E. Glinsky, B. A. Hammel, P. Lee, P. A. Norreys, and M. Tatarakis, Phys. Plasmas 4, 447 (1997).
[47] P. Gibbon, Short Pulse Laser Interactions with Matter: An Introduction (World Scientific, London, 2005)
[48] A. Link, R.R. Freeman, D.W. Schumacher, and L.D. Van Woerkom, Phys. Plasmas 18, 53107 (2011).
[49] H. Sawada, Y. Sentoku, A. Bass, B. Griffin, R. Pandit, F. Beg, H. Chen, H. McLean, A.J. Link, P.K. Patel, and Y. Ping, J. Phys. B At. Mol. Opt. Phys. 48, 224008 (2015)
[50] H. Chen, B. Soom, B. Yaakobi, S. Uchida, and D.D. Meyerhofer, Phys. Rev. Lett. 70, 3431 (1993).
[51] D. Duston, R.W. Clark, J. Davis, and J.P. Apruzese, Phys. Rev. A 27, 1441 (1983).
[52] See Supplemental Material at [url] for determination of the origin of x-ray emission lines and a discussion on cold Kα spectra, which includes Refs. 53 and 54
[53] A. Schönlein, G. Boutoux, S. Pikuz, L. Antonelli, D. Batani, A. Debayle, A. Franz, L. Giuffrida, J.J. Honrubia, J. Jacoby, D. Khaghani, P. Neumayer, O.N. Rosmej, T. Sakaki, J.J. Santos, and A. Sauteray, EPL (Europhysics Lett. 114, 45002 (2016).
[54] A. C. Thompson and D. Vaughan, X-ray Data Booklet, 3rd ed., Lawrence Berkeley National Laboratory (2009)
[55] J. A. Koch, Y. Aglitskiy, C. Brown, T. Cowan, R. Freeman, S. Hatchett, G. Holland, M. Key, A. MacKinnon, J. Seely, R. Snavely, and R. Stephens, Rev. Sci. Instrum. 74, 2130 (2003).
[56] J. A. King, K. Akli, B. Zhang, R. R. Freeman, M. H. Key, C. D. Chen, S. P. Hatchett, J. A. Koch, A. J. MacKinnon, P. K. Patel, et al., Appl. Phys. Lett. 86, 191501 (2005).
[57] K.U. Akli, M.H. Key, H.K. Chung, S.B. Hansen, R.R. Freeman, M.H. Chen, G. Gregori, S. Hatchett, D. Hey, N. Izumi et al., Phys. Plasmas 14, 023102 (2007).
[58] W. Theobald, A. A. Solodov, C. Stoeckl, K. S. Anderson, F. N. Beg, R. Epstein, G. Fiksel, E. M. Giraldez, V. Y. Glebov, H. Habara, et al., Nat. Commun. 5, 5785 (2014).
[59] H. Sawada, S. Lee, T. Shiroto, H. Nagatomo, Y. Arikawa, H. Nishimura, T. Ueda, K. Shigemori, A. Sunahara, N. Ohnishi, et al., Appl. Phys. Lett. 108, 254101 (2016).
[60] See Supplemental Material at [url] for a discussion on ionization-dependent spectra and variation of the x-ray intensity within the crystal bandwidth, which includes Ref. 61.
[61] J. J. MacFarlane, I. E. Golovkin, and P. R. Woodruff, internal report, PCS-R-113 (2010)
[62] See Supplemental Material for close-up views of the x-ray images.
[63] National Institute of Standards and Technology, 2010, "ESTAR, Stopping Power and Range Tables for Electrons," (http://physics.nist.gov/PhysRefData/Star/Text/ESTAR.html)
[64] J. Myatt, W. Theobald, J.A. Delettrez, C. Stoeckl, M. Storm, T.C. Sangster, A. V. Maximov, and R.W. Short, Phys. Plasmas 14, 056301 (2007).
[65] See Supplemental Material at [url] for a discussion on Kα spectral analysis and alternative interpretation of the data
[66] W. Schulz, U. Eppelt, and R. Poprawe, J. Laser Appl. 25, 012006 (2013).
[67] D. Salzmann, Atomic Physics in Hot Plasmas (Oxford University, New York, 1998), P.72
[68] K. Eidmann, U. Andiel, F. Pisani, P. Hakel, R.C. Mancini, G.C. Junkel-Vives, J. Abdallah, and K. Witte, J. Quant. Spectrosc. Radiat. Transf. 81, 133 (2003).
[69] See Supplemental Material at [url] for the PICLS simulation setup, which includes Ref. 70.
[70] J. J. MacFarlane, I.E. Golovkin, and P.R. Woodruff, J. Quant. Spectrosc. Radiat. Transf. 99, 381 (2006)
[71] See Supplemental Material at [url] for phase maps of fast electrons and ions at 0.5, 1.0, 1.5 and 2.0 ps.
[72] Y. Sentoku, T.E. Cowan, A. Kemp, and H. Ruhl, Phys. Plasmas 10, 2009 (2003)
[73] See Supplemental Material at [url] for PrismSPECT model, comparisons of data with model at 1.0, 1.5, 2.0 ps.
[74] L.C. Jarrott, M.S. Wei, C. McGuffey, A.A. Solodov, W. Theobald, B. Qiao, C. Stoeckl, R. Betti, H. Chen, J. Delettrez, et al., Nat. Phys. 12, 499 (2016).
[75] S. Sakata, S. Lee, H. Morita, T. Johzaki, H. Sawada, Y. Iwasa, K. Matsuo, K.F.F. Law, A. Yao, M. Hata et al, Nat. Commun. 9, 3937 (2018).